

Transverse and Temporal Characteristics of a High-Gain Free-Electron Laser in the Saturation Regime^{*}

Zhirong Huang¹, Kwang-Je Kim

Advanced Photon Source, Argonne National Laboratory, Argonne, IL 60439, USA

Abstract

The transverse and the temporal characteristics of a high-gain free-electron laser are governed by refractive guiding and sideband instability, respectively. Using the self-consistent Vlasov-Maxwell equations, we explicitly determine the effective index of refraction and the guided radiation mode for an electron beam with arbitrary transverse size. Electrons trapped by the guided radiation execute synchrotron oscillation and hence are susceptible to the sideband instability. We explain the spectral evolution and determine the sideband growth rate. These theoretical predictions agree well with GINGER simulation results.

Key words: free-electron laser, saturation, refractive guiding, sideband instability

PACS: 41.60.Cr

1 Introduction

After an initial start-up stage and an exponential buildup, the radiation power of a high-gain free-electron laser (FEL) saturates. A future light source facility based on a high-gain FEL is very likely to operate in the saturation regime for maximum power extraction and high stability. This paper investigates

^{*} Work supported by the U. S. Department of Energy under Contract No. W-31-109-ENG-38.

¹ Corresponding author. Tel: (630)252-6023; Fax: (630)252-5703; Email: zrh@aps.anl.gov

both the transverse and the temporal characteristics of the radiation in the saturation regime.

It is worthwhile to first summarize the radiation characteristics in the exponential growth regime. In the transverse domain, the interplay between diffraction and gain usually selects a single transverse mode that has a larger growth rate than any other modes [1]. This process is referred as *gain guiding*. In the temporal or frequency domain, an initially broadband spectrum of white noise (in the case of self-amplified spontaneous emission (SASE)) becomes narrower as the gain is predominant near the resonant frequency [2].

In the saturation regime, the electrons are trapped in the ponderomotive potential of the combined radiation and undulator fields. Scharlemann *et al.* uses a fiber analog to point out that guided transverse modes can exist due to the effective index of refraction caused by the FEL interaction [3]. This process may be referred as *refractive guiding*. In this paper, we study the refractive guiding with the self-consistent Vlasov-Maxwell equations and compare the results with the FEL simulation code GINGER [4]. The equilibrium state formed by the guided radiation and the trapped electrons is unstable in the presence of sideband waves [5]. We discuss the sideband instability and its implications to SASE FELs.

2 Refractive Guiding

For simplicity, we consider a parallel electron beam by ignoring the transverse betatron motion. The electron motion is governed by the pendulum equation

$$\frac{d\theta}{d\bar{z}} = \bar{\eta}, \quad \frac{d\bar{\eta}}{d\bar{z}} = -a(\bar{\mathbf{x}}, \tau; \bar{z}) \exp(i\theta) + \text{c.c.}, \quad (1)$$

where $\bar{z} = 2\rho k_u z$ is the scaled distance in an undulator with period $\lambda_u = 2\pi/k_u$, θ is the electron phase relative to the resonant wave $\exp(ik_r z - i\omega_r t)$, $\bar{\eta} = \delta\gamma/(\gamma\rho)$ is the scaled electron energy, $\bar{\mathbf{x}} = \mathbf{x}\sqrt{2\rho k_r k_u}$ and $\tau = 2\rho\omega_r(\delta t)$ are the scaled transverse and temporal coordinates, and a is the scaled slowly varying electric field. Here ρ is the FEL scaling parameter [6].

At FEL saturation, we may assume the radiation has established a dominant frequency component at, say, ω_r . The radiation power stays approximately constant along \bar{z} after saturation, but both the amplitude and phase of the radiation field can vary with \bar{z} . Following Refs. [7,8], we look for a “primary wave” of the form

$$a_0(\bar{\mathbf{x}}; \bar{z}) = A(\bar{\mathbf{x}})e^{i\kappa\bar{z} + \phi_0}. \quad (2)$$

Electron motion under such a field is governed by a stationary Hamiltonian

$$H_0 = \frac{1}{2}\psi'^2 - 2A(\bar{\mathbf{x}})\sin\psi, \quad (3)$$

where $\psi = \theta + \kappa\bar{z} + \phi_0$ and $\psi' = \bar{\eta} + \kappa$ are canonical variables. The electron distribution function that satisfies the Vlasov equation is $F_0(H_0)U(\bar{\mathbf{x}})$, where F_0 is an arbitrary function of H_0 , and $U(\bar{\mathbf{x}})$ describes the transverse profile of the electron beam.

The computer simulation of Ref. [8] shows that the electron distribution in the saturation regime is very similar to the Boltzmann distribution

$$F_0(H_0) = \frac{\sqrt{\xi}}{\sqrt{2\pi}I_0(2\xi A)}e^{-\xi H_0}, \quad (4)$$

where I_m is the modified Bessel function of order m , and ξ is a measure of particle spread in the ponderomotive potential. Under these assumptions, the paraxial wave equation for the “primary wave” becomes

$$\left(\kappa - \frac{1}{2}\frac{\partial^2}{\partial\bar{\mathbf{x}}^2}\right)A(\bar{\mathbf{x}}) = U(\bar{\mathbf{x}})\frac{I_1(2\xi A)}{I_0(2\xi A)} \approx \xi U(\bar{\mathbf{x}})A(\bar{\mathbf{x}}). \quad (5)$$

The ratio of the modified Bessel functions is the bunching fraction. To be consistent with the last approximation, we require that $\xi A < 1$. The approximated equation can be shown to be equivalent to the mode equation in optical fibers [9] with the effective index of refraction

$$n \equiv 1 + \frac{2\rho k_u}{k_r} \xi U(\bar{\mathbf{x}}). \quad (6)$$

Generated by the bunched electron beam, this effective index of refraction is slightly larger than 1 and can guide the radiation after saturation [3]. To demonstrate refractive guiding, we apply Snell's law from geometrical optics [9] to obtain the critical angle for total internal reflection:

$$\theta_c \approx \sqrt{2(n-1)} = \sqrt{\frac{\xi U(\bar{\mathbf{x}})}{\pi\sqrt{3}} \frac{\lambda_r}{L_G^0}}. \quad (7)$$

Here $L_G^0 = \lambda_u/(4\pi\sqrt{3}\rho)$ is the one-dimensional (1-D) power gain length in the exponential growth regime, and $\xi \sim 1$ after saturation. The right-hand side of Eq. (7) is approximately the radiation angle determined by gain guiding. Thus, the radiation is expected to be confined to the e-beam due to the total internal reflection.

We take a round, uniform electron beam with a transverse size R (i.e., $U(\bar{\mathbf{x}}) = 1$ when $|\bar{\mathbf{x}}| \equiv \bar{r} < \bar{R} \equiv R\sqrt{2k_r k_u \rho}$ and zero otherwise). Since the guided mode in the exponential region is axisymmetric, we look for the axisymmetric solution that satisfies Eq. (5):

$$A(\bar{r}) = \begin{cases} A_0 J_0(\sqrt{2(\xi - \kappa)}\bar{r}) & \bar{r} < \bar{R}, \\ A_0 \frac{J_0(\sqrt{2(\xi - \kappa)}\bar{R})}{K_0(\sqrt{2\kappa}\bar{R})} K_0(\sqrt{2\kappa}\bar{r}) & \bar{r} > \bar{R}, \end{cases} \quad (8)$$

where J_m and K_m are the usual Bessel functions of order m . Matching at $\bar{r} = \bar{R}$ yields:

$$\frac{y_1 J_1(y_1)}{y_2 J_0(y_1)} = \frac{K_1(y_2)}{K_0(y_2)}, \quad (9)$$

where $y_1 \equiv \sqrt{2(\xi - \kappa)\bar{R}}$ and $y_2 \equiv \sqrt{2\kappa\bar{R}}$. As pointed out in Ref. [8], the equilibrium solutions are constrained by two constants of motion concerning the first and second moments of electron energy distribution:

$$\begin{aligned}\kappa &= \frac{\int d\bar{\mathbf{x}} A^2(\bar{\mathbf{x}})}{\int d\bar{\mathbf{x}} U(\bar{\mathbf{x}})} \quad (\text{energy conservation}), \\ \xi^{-1} &= \frac{\sigma_{\eta 0}^2}{\rho^2} + 3\kappa^2 + \frac{\int d\bar{\mathbf{x}} |\partial A / (\partial \bar{\mathbf{x}})|^2}{\int d\bar{\mathbf{x}} U(\bar{\mathbf{x}})},\end{aligned}\quad (10)$$

where $\sigma_{\eta 0} = (\sigma_\gamma / \gamma)_0$ is the initial rms energy spread. Putting Eq. (8) into Eq. (10) and eliminating A_0 , we obtain

$$\begin{aligned}\frac{2\bar{R}^2}{y_1^2 + y_2^2} &= \frac{\sigma_{\eta 0}^2}{\rho^2} + \frac{y_2^4}{4\bar{R}^4} + \frac{(y_1^2 + y_2^2)y_2^2}{2\bar{R}^4} \\ &\times \frac{J_0^2(y_1) + J_1^2(y_1)}{J_0^2(y_1) + J_1^2(y_1) + J_0^2(y_1)/y_2}.\end{aligned}\quad (11)$$

Given the electron beam size R and the initial energy spread $\sigma_{\eta 0}$, Eqs. (9) and (11) can be solved numerically to determine y_1 and y_2 , and hence κ , ξ , and the guided mode $A(r)$. The mode profile that satisfies the consistency requirement $\xi A_0 < 1$ is that of TEM₀₀ (nodeless). As $\sigma_{\eta 0} = 0$ and $R \rightarrow \infty$, we have $\xi = \kappa \approx 0.7$ with the plane wave solution, in agreement with Ref. [8] obtained using a longitudinal phase-space model that is a delta function in H_0 . There appears to be a systematic difference between the two models in the limit $R \rightarrow 0$.

Let us compare the theory with the GINGER [4] simulations employing a parallel electron beam with a Gaussian transverse profile (rms size σ_x). We take $R = \sqrt{2}\sigma_x$ and use the relations

$$\begin{aligned}\kappa &= \frac{1}{2\rho k_u} \frac{d\phi}{dz} = \frac{P_s}{\rho P_{\text{beam}}}, \\ \xi^{-1} + \kappa^2 &= \int \frac{d\theta}{2\pi} \int d\bar{\eta} \bar{\eta}^2 F(H_0) = \frac{\sigma_{\eta s}^2}{\rho^2},\end{aligned}\quad (12)$$

where ϕ is the phase of the “primary wave,” P_{beam} is the electron beam power, P_s is the equilibrium radiation power after saturation, and σ_{η_s} is the equilibrium energy spread after saturation. As shown in Fig. 1, κ obtained from Eqs. (9) and (11) for $\sigma_{\eta_0} = 0$ agrees well with the simulation results obtained from the radiation phase (at $r = 0$) and from the average power level after saturation (see Eq. (12)). In Fig. 2 the equilibrium energy spread in units of ρ is obtained through the theory ($= \sqrt{\xi^{-1} + \kappa^2}$) and through simulations. Although the theory predicts correctly the rising σ_{η_s} with increasing R , the numerical values are higher than the simulation results, implying the electron longitudinal phase space is more complicated than the simple Boltzmann distribution used in the theory.

Next, we examine the evolution of the transverse profile after saturation. After an initial overshoot in the radiation power at the onset of saturation, the beam-radiation system tends to relax to the self-consistent equilibrium state prescribed above. Some of the excess radiation is unguided and “leaks” out of the electron beam through diffraction, while the rest of the excess radiation gives rise to small amplitude and phase oscillations around the equilibrium state [8]. Figure 3 illustrates these transverse characteristics using the GINGER simulation of the low-energy undulator test line (LEUTL) FEL [10] at the Advanced Photon Source. The increase of the rms transverse size of the radiation with distance z can be explained by the “leaking” portion of the radiation propagating to $r \rightarrow \infty$, and the (almost) constant FWHM transverse size clearly indicates a well-guided transverse mode. In Fig. 4, we show comparison between the calculated FWHM transverse size as a function of \bar{R} ($\sigma_{\eta_0} = 0$) and the GINGER simulation results using a parallel electron beam. The agreement is again good. Note that our analysis does not take into account the e-beam emittance ε and is expected to be valid when $\varepsilon < \lambda_r/(4\pi)$.

3 Sideband instability

As shown in Sec. 2, electrons subject to the Hamiltonian of Eq. (3) execute synchrotron oscillation in the ponderomotive potential formed by the “primary wave” and the undulator magnetic field. The small-amplitude synchrotron frequency is given by $\Omega_0 = 2\rho\omega_r\sqrt{2A}$. Thus, a wave that is shifted from the resonant frequency by an amount equal to Ω_0 can interact resonantly with the synchrotron motion and give rise to the sideband instability [5]. This instability has been studied extensively in the literature, including Refs. [7] and many others. However, there has been some confusion that the calculated growth spectra is symmetric about the “primary wave” frequency, while simulations indicate that the spectrum is asymmetric towards the lower sidebands [7].

Following the one-dimensional analysis of Ref. [11], we write the temporal electric field as

$$a(\tau; \bar{z}) = a_0(\bar{z}) + \int d\bar{\nu} b_{\bar{\nu}}(\bar{z}) e^{i\bar{\nu}\tau} e^{i\kappa\bar{z} + \phi_0 - i\bar{\nu}\bar{z}}, \quad (13)$$

where $a_0(\bar{z})$ is the equilibrium solution (i.e., Eq. (2)), $\bar{\nu}$ is the scaled detuning (i.e., $\omega = \omega_r(1 - 2\rho\bar{\nu})$), and $b_{\bar{\nu}}$ is a sideband wave and is treated as a perturbation. Linearizing the Vlasov-Maxwell equations and assuming $b_{\bar{\nu}} \propto e^{\Gamma_{\bar{\nu}}\bar{z}}$, one obtain [11]

$$\Gamma_{\bar{\nu}} = \sqrt{[\alpha_{\bar{\nu}} + i(\delta_0 - \kappa)]^2 - (\beta_{\bar{\nu}} + i\delta_2)^2}. \quad (14)$$

where

$$\begin{aligned} \delta_n &\approx \int_0^{2\pi} \frac{d\theta}{2\pi} \int_{-\infty}^{\infty} d\bar{\eta} \cos(n\psi) \frac{dF_0}{dH_0}, \quad n = 0, 2, \\ \alpha_{\bar{\nu}} &\approx -8\sqrt{2A}F_0'(2A)f\left(\frac{|\bar{\nu}|}{\sqrt{2A}}\right), \\ \beta_{\bar{\nu}} &\approx -8\sqrt{2A}F_0'(2A)g\left(\frac{|\bar{\nu}|}{\sqrt{2A}}\right), \end{aligned} \quad (15)$$

and $f(x)$ and $g(x)$ are lineshape functions defined in Ref. [11] (neglecting the untrapped-particle contributions). The corresponding eigenmode is a mixture of both lower and upper sidebands that satisfies

$$[\Gamma_{\bar{\nu}} - \alpha_{\bar{\nu}} - i(\delta_0 - \kappa)]b_{\bar{\nu}} = (\beta_{\bar{\nu}} + i\delta_2)b_{(-\bar{\nu})}^*. \quad (16)$$

In general, $|\beta_{\bar{\nu}} + i\delta_2| \ll |\alpha_{\bar{\nu}} - i(\delta_0 - \kappa)|$, hence we have $|b_{\bar{\nu}}| \gg |b_{(-\bar{\nu})}|$ for $\bar{\nu} > 0$. The FEL spectrum after saturation always contains more lower sidebands than upper sidebands even though the growth rates of both sidebands are equal.

A physical picture of the spectral behavior after saturation was discussed in Ref. [12]: an initially symmetric spectrum can be viewed as a frequency-modulated wave. The lower frequency portion of such a wave can extract more energy because the electron is farther above the resonance, while the opposite is true for the upper frequency portion of the wave. As a result, the frequency and the amplitude modulation become correlated, and the spectrum is asymmetric, emphasizing the lower sidebands (longer wavelength) at the expense of the upper sidebands. As the energy is continuously extracted, the sidebands grow and the spectral width becomes broader.

For numerical calculation, let us first consider the zero detuning case ($\bar{\nu} = 0$). Using the Boltzmann distribution for F_0 (Eq. (4)) and the self-consistent 1-D equilibrium solution ($-\delta_0 = \xi = \kappa = A^2 = 0.7$), we have $\Gamma_0 \approx 2i\kappa = 1.4i$, since $\alpha_0 = \beta_0 = 0$ and $|\delta_2| \ll |\delta_0|$. Thus, the power of the “primary wave” is oscillatory around the equilibrium value with a scaled oscillation wavenumber 1.4, comparable to 1.25 observed in 1-D simulations and 1.14 calculated using a different model [8]. For the sideband instability, if we ignore $\beta_{\bar{\nu}}$ and δ_2 in Eq. (14) and take the maximum value of the lineshape function $f(x) \approx 0.56$ at $x = 1$ or $\bar{\nu} = \sqrt{2A} \approx 1.3$ ($\delta\omega = 2.6\rho\omega_r = \Omega_0$), we obtain the maximum

sideband growth rate $Re[\Gamma]_{max} \approx \alpha_1 = 0.30$, or a maximum sideband power gain length

$$L_G^{SB} = \frac{1.7\lambda_u}{4\pi\rho} \approx 3L_G^0. \quad (17)$$

This gain length agrees with the GINGER sideband simulation within 10%.

4 Discussion

The present analysis of refractive guiding and sideband instability assumes a dominant frequency component at a particular frequency and hence is directly applicable to a high-gain FEL amplifier that starts with a coherent seed. For a SASE FEL that starts from the shot noise, the linewidth at the saturation point is about ρ [2], smaller than the location of the strongest sideband component, which is $\sim 2\rho$ away from the resonant frequency. Thus, we expect these physics phenomena to occur in an average sense. For example, after integrating over the temporal dependence, the GINGER SASE simulation of the radiation profile evolves qualitatively as does the GINGER steady-state simulation. Because of the sideband instability, the SASE radiation power continues to grow (slowly) after saturation but at the expense of increased spectral bandwidth. These features have been observed in simulations and may explain some of the spectral measurements at the LEUTL FEL [13,14].

We thank S. Milton and W. Fawley for stimulating discussions, and thank W. Fawley for providing many useful features in GINGER to enable direct comparisons with our analysis.

References

- [1] G.T. Moore, Nucl. Instr. and Meth. A **239**, 19, (1985).

- [2] K.-J. Kim, Nucl. Instr. and Meth. A **250**, 396, (1986). J.-M. Wang and L.-H. Yu, *ibid*, 484 (1986).
- [3] E.T. Scharlemann, A.M. Sessler and J.S. Wurtele, Phys. Rev. Lett. **54**, 1925 (1985).
- [4] W.M. Fawley, CBP Tech Note-104, Lawrence Berkeley Laboratory, 1995.
- [5] N.M. Kroll, P.L. Morton, and M.R. Rosenbluth, IEEE J. Quantum Electron., **QE-17**, 1436 (1981).
- [6] R. Bonifacio, C. Pellegrini, and L.M. Narducci, Opt. Comm. **50**, 373 (1984).
- [7] W.M. Sharp and S.S. Yu, Phys. Fluids B **2**, 581 (1990).
- [8] R.L. Gluckstern, S. Krinsky and H. Okamoto, Phy. Rev. E **47**, 4412 (1993).
- [9] See, for example, D. Marcuse, *Theory of Dielectric Optical Waveguides* (Academic Press, Boston, 1991).
- [10] S. Milton *et al.*, Science **292**, 2037 (2001).
- [11] J.N. Elgin, Phy. Rev. A **43**, 2514 (1991).
- [12] R.W. Warren, J.C. Goldstein, and B.E. Newnam, Nucl. Instr. and Meth. A **250**, 19 (1986).
- [13] A. Lumpkin *et al.*, these proceedings.
- [14] V. Sajaev *et al.*, these proceedings.

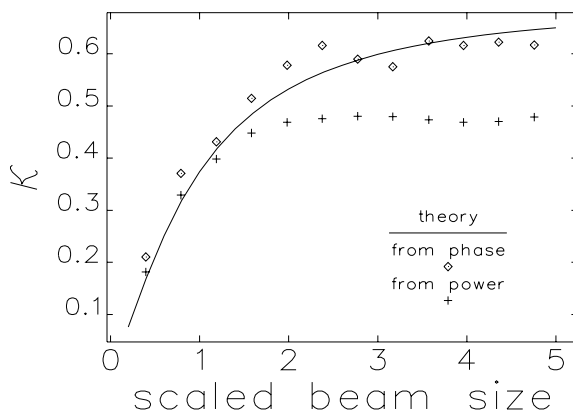


Fig. 1. κ versus the scaled e-beam size \bar{R} as calculated from theory (curve) and from GINGER simulations (symbols) (see text for details.)

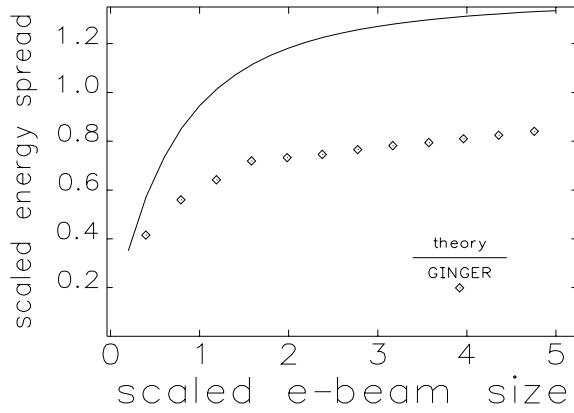


Fig. 2. Equilibrium energy spread in units of ρ .

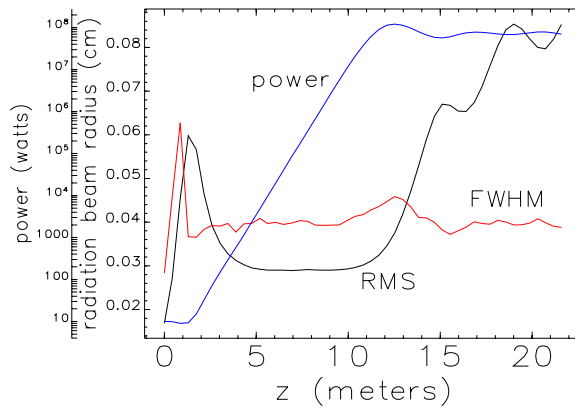


Fig. 3. GINGER steady-state simulation of the LEUTL FEL ($\lambda_r = 530$ nm, $\sigma_{\eta 0} = 0.1\%$ at 217 MeV, peak current 266 A and $\gamma\varepsilon = 8.5\mu\text{m}$).

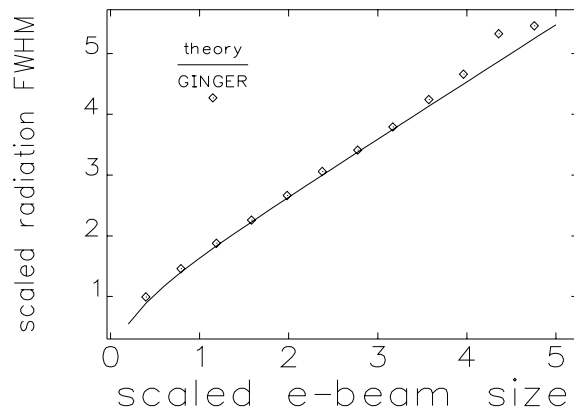


Fig. 4. Scaled FWHM of the radiation transverse size.